# Estimating spatially distributed soil water content at small watershed scales based on decomposition of temporal anomaly and time stability analysis

Wei Hu, Bing Cheng Si

*University of Saskatchewan, Department of Soil Science, Saskatoon, SK S7N 5A8, Canada*

## Abstract

Soil water content (SWC) is crucial to rainfall-runoff response at the watershed scale. A model was used to decompose the spatiotemporal SWC into a time-stable pattern (i.e, temporal mean), a space-invariant temporal anomaly, and a space-variant temporal anomaly. The space-variant temporal anomaly was further decomposed using the empirical orthogonal function (EOF) for estimating spatially distributed SWC. This model was compared to a previous model that decomposes the spatiotemporal SWC into a spatial mean and a spatial anomaly, with the latter being further decomposed using the EOF. These two models are termed temporal anomaly (TA) model and spatial anomaly (SA) model, respectively. We aimed to test the hypothesis that underlying (i.e., time-invariant) spatial patterns exist in the space-variant temporal anomaly at the small watershed scale, and to examine the advantages of the TA model over the SA model in terms of the estimation of spatially distributed SWC. For this purpose, a dataset of near surface (0–0.2 m) and root zone (0–1.0 m) SWC, at a small watershed scale in the Canadian prairies, was analyzed. Results showed that underlying spatial patterns exist in the space-variant temporal

anomaly because of the permanent controls of “static” factors such as depth to the $CaCO_3$ layer and organic carbon content. Combined with time stability analysis, the TA model improved the estimation of spatially distributed SWC over the SA model, especially for dry conditions. Further application of these two models demonstrated that the TA model outperformed the SA model at a hillslope in the Chinese Loess Plateau, but the performance of these two models in the GENCAI network (~250 km²) in Italy was equivalent. The TA model has potential to construct a spatially distributed SWC at small watershed scales from remote sensed SWC.

Keywords: Soil moisture; Soil water downscaling; Empirical orthogonal function; Statistical models; Time stability

## 1. Introduction

Soil water content (SWC) of surface soils exerts a major influence on a series of hydrological processes such as runoff and infiltration (Famiglietti et al., 1998; Vereecken et al., 2007; She et al., 2013a). Soil water content in the root zone is, in many cases, linked to vegetative growth (Wang et al., 2012; Ward et al., 2012; Jia and Shao, 2013). Obtaining accurate information on the spatiotemporal SWC is crucial for improving hydrological prediction and soil water management (Venkatesh et al., 2011; Champagne et al., 2012; She et al., 2013b; Zhao et al., 2013). While remote sensing has advanced SWC measurements of surface soils (<5 cm thick) at basin (2,500–25,000 $km^2$) and continental scales (Robinson et al., 2008), characterization of spatially distributed SWC at small watershed (0.1–80 $km^2$) scales still poses a

43 challenge. A method is needed for estimating spatially distributed SWC in the near
44 surface and root zone at watershed scales.

45 Time stability of SWC, which refers to similar spatial patterns of SWC across
46 different measurement times (Vachaud et al., 1985; Brocca et al., 2009), has been used
47 for estimating spatially distributed SWC (Starr, 2005; Perry and Niemann, 2007;
48 Blöschl et al., 2009). This method is conceptually-appealing, but assumes completely
49 time-stable spatial patterns of SWC.

50 The time-stable pattern does not explain all of the spatial variances in SWC,
51 indicating the existence of time-variant components (Starr, 2005). In order to identify
52 underlying patterns of SWC that have time-variant components, the spatiotemporal
53 SWC was decomposed into a spatial mean and a spatial anomaly. The spatial anomaly
54 of the SWC was further decomposed into the sum of the product of time-invariant
55 spatial patterns (EOFs) and temporally varying, but spatially constant coefficients
56 (ECs) using the empirical orthogonal function (EOF) (Fig. 1) (Jawson and Niemann,
57 2007; Perry and Niemann, 2007, 2008; Joshi and Mohanty, 2010; Korres et al., 2010;
58 Busch et al., 2012). Spatially distributed SWC estimates based on the decomposition
59 of spatial anomaly outperformed those based on time-stable patterns (Perry and
60 Niemann, 2007).

61 Recently, the spatiotemporal SWC was also decomposed into a temporal mean and
62 a temporal anomaly (Mittelbach and Seneviratne, 2012) (Fig. 1). Previous studies
63 indicated that the contribution of the temporal anomaly to the total spatial variance
64 was notable (Mittelbach and Seneviratne, 2012; Brocca et al., 2014; Rötzer et al.,

65 2015). These studies, however, only focused on surface soils at large scales (> 250
66 $km^2$). Vanderlinden et al. (2012) suggested that the temporal mean may be further
67 decomposed into its spatial mean and residuals, and the temporal anomaly may be
68 further decomposed into space-invariant term (i.e., spatial mean of temporal anomaly)
69 and space-variant term (i.e., spatial residuals of temporal anomaly) (Fig. 1). Note that
70 the spatial variance in the temporal anomaly (Mittelbach and Seneviratne, 2012)
71 equals that of the space-variant term of the temporal anomaly (Vanderlinden et al.,
72 2012). The further decomposition of the temporal anomaly may be physically
73 meaningful, because the space-invariant and space-variant terms in the temporal
74 anomaly may be forced differently. However, the models of Mittelbach and
75 Seneviratne (2012) and Vanderlinden et al. (2012) have not been used for estimating
76 spatially distributed SWC. If the space-variant terms are ignored during the estimation
77 of spatially distributed SWC, their models are equivalent to that based on time-stable
78 patterns. Therefore, estimation of spatially distributed SWC may be improved by
79 incorporating the space-variant term of the temporal anomaly if underlying (i.e.,
80 time-invariant) spatial patterns exist in the temporal anomaly.

81 To our knowledge, the importance of the space-variant term of the temporal
82 anomaly and its physical meaning at small watershed scales is not well-known. Based
83 on previous studies (Perry and Niemann, 2007; Mittelbach and Seneviratne, 2012;
84 Vanderlinden et al., 2012), we assume soil water dynamics at watershed scales can be
85 decomposed into three components (Fig. 1): (1) time-stable pattern (i.e., temporal
86 mean, spatial forcing): the “static” factors such as soil and topography control the

pattern; (2) space-invariant temporal anomaly (temporal forcing): the "dynamic" factors such as meteorological variables and vegetation change with time, and therefore modify SWC in time, regardless of spatial locations; and (3) space-variant temporal anomaly (interactions between spatial forcing and temporal forcing): this term represents interactions between "static" and "dynamic" factors. For example, SWC recharge introduced by a rainfall may be modified by topography through runoff processes; SWC loss triggered by evapotranspiration may be regulated by topography through solar radiation exposure.

The "static" factors may be persistent in the space-variant temporal anomaly, and their impacts on the space-variant temporal anomaly likely change with time. Thus, we hypothesize that some underlying (i.e., time-invariant) spatial patterns exist in the space-variant temporal anomaly, and their impacts can be modulated by a time coefficient, both of which can be obtained by the EOF method (Fig. 1). If the hypothesis is true, the estimation of spatially distributed SWC utilizing the EOF decomposition may outperform the one suggested by Perry and Niemann (2007). This is because: (1) the spatial anomaly which was decomposed using the EOF in Perry and Niemann (2007) lumped the time-stable pattern and space-variant temporal anomaly together (Fig. 1); (2) the underlying spatial patterns in the spatial anomaly may not fully capture both time-stable patterns and patterns in the space-variant temporal anomaly due to the possible nonlinear relations between these two terms.

Therefore, the objectives were (1) to test the hypothesis that underlying spatial patterns exist in the space-variant temporal anomaly at small watershed scales and (2)

to examine whether the decomposition of the space-variant temporal anomaly using the EOF has any advantages over the decomposition of the spatial anomaly (Perry and Niemann, 2007) for estimating spatially distributed SWC. Two steps were included in the estimation of spatially distributed SWC. First, the spatial mean SWC was upscaled from the SWC measurement at the most time-stable location using time stability analysis. Following this, the spatially distributed SWC was downscaled from the estimated spatial mean SWC. For the purpose of this study, spatiotemporal SWC datasets at depths of near surface (0–0.2 m) and root zone (0–1.0 m) from a Canadian prairie landscape were used. Spatiotemporal SWC of samples taken 0–0.06 m from a hillslope (100 m) in the Chinese Loess Plateau and 0–0.15 m from the GENCAI network (~250 km²) in Italy were also used to further demonstrate conditions under which the decomposition of the spatial anomaly was beneficial to the estimation of spatially distributed SWC.

# 2. Materials and methods

## 2.1 Study area and data collection

This study was conducted in the Canadian prairie pothole region at St. Denis National Wildlife Area (52°12′ N, 106°50′ W) with an area of 3.6 $km^2$. This area has a humid continental climate (Peel et al., 2007), and had a mean annual air temperature of 1.9 °C and a mean annual precipitation of 402 mm during the study period (Fig. 2). A variety of depressions, knolls, and knobs result in a sequence of undulating slopes (Biswas et al., 2011). The elevation varies from 554.8 to 557.5 m. The soils are

dominated by clay loam textured Mollisols (Soil Survey Staff, 2010) and covered by mixed grass, i.e., smooth brome grass (*Bromus inermis*) and alfalfa (*Medicago sativa* L.). The near surface soil porosity ranges from 38% (knolls) to 70% (depressions). Calcium carbonates ($CaCO_3$) derived mostly from fragments of limestone rocks are common in the Canadian Prairies. The $CaCO_3$ is dissolved by the slightly acidic rainwater moving through the upper horizons and deposited to lower horizons. The heterogeneous amount of infiltrated water resulted in a varying depth of $CaCO_3$ layer ranging from almost 0 m in the knolls to 2.1 m in the depressions. A 576 m long sampling transect with 128 sampling locations spaced at 4.5 m intervals was established over several rounded knolls and depressions. At each location, a time domain reflectometry probe was used to measure SWC of the near surface soil (0–0.2 m), and a neutron probe was used to collect SWC measurements at 0.2 m intervals between a depth of 0.2 and 1.0 m. The SWC was measured on a volumetric basis and expressed as a percentage (%) volume of water per unit soil volume. The SWC of the root zone was calculated by averaging the SWC of 0–0.2, 0.2–0.4, 0.4–0.6, 0.6–0.8, and 0.8–1.0 m. Soil water content was measured on 23 dates from July 17, 2007 to September 29, 2011. The SWC dataset was collected in all seasons except winter, and accurately portrays the variations in soil water conditions in the study area. In addition to the SWC dataset, the soil, vegetative, and topographical properties were obtained at each sampling location. These properties included soil particle components (clay, silt, and sand contents), bulk density, soil organic carbon (SOC) content for the surface layer, A horizon depth, C horizon depth, depth to the $CaCO_3$ layer, leaf area index,

elevation, cos(aspect), slope, curvature, gradient, upslope length, solar radiation, specific contributing area, convergence index, wetness index, and flow connectivity. Detailed information on the measurements can be found in Biswas et al. (2012).

### 2.2 Statistical models for decomposing soil water content

Spatiotemporal SWC at small watershed scales was decomposed into three components: time-stable pattern, space-invariant temporal anomaly, and space-variant temporal anomaly. This model was compared to the one that decomposed SWC into spatial mean and spatial anomaly (Perry and Niemann, 2007). Both the space-variant temporal anomaly and spatial anomaly were decomposed using the EOF method. The two models are termed temporal anomaly (TA) model and spatial anomaly (SA) model, respectively. Figure 1 displays the differences between the two models. Each component will be explained in detail later. The explanation of nomenclatures is listed in Table A1. Because we focus on estimating spatial distribution of SWC at any given time, only spatial variances of SWC were taken into account. Therefore, the variance or covariance denotes the quantity in space without specifications.

#### 2.2.1 The SA model

Perry and Niemann (2007) expressed SWC at location $n$ and time $t$ ($S_{tn}$) as (Fig. 1):

$$S_{tn} = S_{t\hat{n}} + Z_{tn}, \qquad (1)$$

where $S_{t\hat{n}}$ is the spatial mean SWC at time $t$ (temporal forcing) and $Z_{tn}$ is the spatial anomaly of SWC (lumped spatial forcing and interactions). The subscript $\hat{n}$ ($\hat{t}$) indicates a space (time) averaged quantity.

According to Perry and Niemann (2007), $S_{t\hat{n}}$ can be estimated by remote sensing,

175 water balance models, and in situ soil water measurement at a representative (or
176 time-stable) location. The in situ soil water measurement method was selected
177 because the representative location can be easily determined with prior SWC datasets.
178 By measuring SWC only at the most time-stable location (*s*) and future time *t* ($S_{ts}$),
179 $S_{t\hat{n}}$ can be estimated using (Grayson and Western, 1998):

180 $$S_{t\hat{n}} = \frac{S_{ts}}{1+\delta_{\hat{ts}}} \quad , \qquad (2)$$

181 where the *s* was identified using the time stability index of mean absolute bias error
182 (Hu et al., 2010, 2012). The $\delta_{\hat{ts}}$ is the temporal mean relative difference of SWC at
183 the *s*, which was calculated with prior measurements.

184 Spatial anomaly ($Z_{tn}$) can be reconstructed by the sum of the product of
185 time-invariant spatial structures (EOFs) and temporally varying coefficients (ECs)
186 using the EOF method (Perry and Niemann, 2007; Joshi and Mohanty, 2010;
187 Vanderlinden et al., 2012). The ECs correspond to the eigenvectors of the matrix of
188 spatial covariance of the $Z_{tn}$, and the EOFs are obtained by projecting the $Z_{tn}$ onto
189 the matrix ECs as: $\mathrm{EOFs} = Z_{tn}\,\mathrm{EC}s$. The number of EOF (or EC) series equals the
190 number of sampling dates. Each EOF series corresponds to one value at each location,
191 and each EC series has one value at each measurement time. Each EOF is chosen to
192 be orthogonal to other EOFs, and the lower-order EOFs account for as much variance
193 as possible. The sum of variances of all EOFs equals the sum of variances of $Z_{tn}$
194 from all measurement times.

195 Usually, a substantial amount of variance can be explained by a small number of
196 EOFs. Johnson and Wichern (2002) suggested the eigenvalue confidence limits

method for selecting the number of EOFs. Once the number of significant EOFs at a confidence level of 95% is selected, $Z_{tn}$ can be estimated as the sum of the product of significant EOFs and associated ECs as:

$$Z_{tn} = \sum \mathrm{EOF}^{sig} \times (\mathrm{EC}^{sig})^{T}, \quad (3)$$

where $\mathrm{EOF}^{sig}$ represents the significant EOFs of the $Z_{tn}$ obtained during model development, $\mathrm{EC}^{sig}$ is the associated temporally varying coefficient, and the superscript *T* represents matrix transpose. Following Perry and Niemann (2007), the associated significant EC at time *t* ($\mathrm{EC}_t$), is estimated by the cosine relationship between EC and $S_{t\hat{n}}$ developed using prior measurements:

$$\mathrm{EC}_t = a + b\cos\left(\frac{2\pi}{c} S_{t\hat{n}} - d\right), \quad (4)$$

where *a*, *b*, *c*, and *d* are the fitted parameters using prior measurements and $S_{t\hat{n}}$ is estimated from Eq. (2). By using the continuous function, $\mathrm{EC}_t$ can be estimated at any $S_{t\hat{n}}$ values, which allows for the estimation of spatially distributed SWC at any soil water conditions.

### 2.2.2 The TA model

Mittelbach and Seneviratne (2012) decomposed the $S_{tn}$ into a time-stable pattern (i.e., temporal mean) and a temporal anomaly component (Fig. 1):

$$S_{tn} = M_{\hat{t}n} + A_{tn}, \quad (5)$$

where $M_{\hat{t}n}$ is the time-stable pattern (spatial forcing) controlled by "static" factors such as soil properties and topography; $A_{tn}$ refers to the temporal anomaly (lumped temporal forcing and interactions). The variance of SWC ($\sigma^2_{\hat{n}}(S_{tn})$) is the sum of variance of the $M_{\hat{t}n}$ ($\sigma^2_{\hat{n}}(M_{\hat{t}n})$), variance of the $A_{tn}$ ($\sigma^2_{\hat{n}}(A_{tn})$), and two times of

219 covariance between $M_{\hat{t}n}$ and $A_{tn}$ ($2\mathrm{cov}(M_{\hat{t}n}, A_{tn})$), which can be expressed as:

220 $$\sigma^2_{\hat{n}}\left(S_{tn}\right) = \sigma^2_{\hat{n}}\left(M_{\hat{t}n}\right) + 2\,\mathrm{cov}(M_{\hat{t}n}, A_{tn}) + \sigma^2_{\hat{n}}\left(A_{tn}\right). \quad (6)$$

221 Because the $A_{tn}$ in Mittelbach and Seneviratne (2012) is a lumped term, it can be
222 further decomposed into space-invariant temporal anomaly ($A_{t\hat{n}}$, i.e., temporal
223 forcing) and space-variant temporal anomaly ($R_{tn}$, i.e., interactions) (Vanderlinden et
224 al., 2012). At a watershed scale, the $A_{t\hat{n}}$ is controlled by temporally varying factors
225 such as meteorological variables and vegetation. Positive and negative $A_{t\hat{n}}$
226 correspond to relatively wet and dry periods, respectively. The $R_{tn}$ refers to the
227 redistribution of $A_{t\hat{n}}$ among different locations due to the interactions between
228 spatial forcing and temporal forcing. For example, soil and topography regulate how
229 much rainfall enters soil and how much water runs off or runs on at a location. This,
230 in turn, dictates vegetation growth in a water-limited environment. Therefore, $S_{tn}$
231 can also be expressed as (Fig. 1):

232 $$S_{tn} = M_{\hat{t}n} + A_{t\hat{n}} + R_{tn}. \quad (7)$$

233 The temporal trends of $A_{t\hat{n}}$ in Eq. (7) and $S_{t\hat{n}}$ in Eq. (1) are the same as both
234 represent temporal forcing. Because the $A_{t\hat{n}}$ is space-invariant and orthogonal to the
235 $M_{\hat{t}n}$ and $R_{tn}$ in a space, $\sigma^2_{\hat{n}}\left(S_{tn}\right)$ in Eq. (6) can also be written as:

236 $$\sigma^2_{\hat{n}}\left(S_{tn}\right) = \sigma^2_{\hat{n}}\left(M_{\hat{t}n}\right) + 2\,\mathrm{cov}(M_{\hat{t}n}, R_{tn}) + \sigma^2_{\hat{n}}\left(R_{tn}\right), \quad (8)$$

237 where $\mathrm{cov}(M_{\hat{t}n}, R_{tn})$ is the covariance between the $M_{\hat{t}n}$ and $R_{tn}$, and $\sigma^2_{\hat{n}}\left(R_{tn}\right)$ is
238 the variance of the $R_{tn}$. Apparently, $2\,\mathrm{cov}(M_{\hat{t}n}, R_{tn})$ equals $2\,\mathrm{cov}(M_{\hat{t}n}, A_{tn})$, and
239 $\sigma^2_{\hat{n}}\left(R_{tn}\right)$ equals $\sigma^2_{\hat{n}}\left(A_{tn}\right)$. The percent (%) contributions of $\sigma^2_{\hat{n}}\left(M_{\hat{t}n}\right)$,
240 $2\,\mathrm{cov}(M_{\hat{t}n}, R_{tn})$, and $\sigma^2_{\hat{n}}\left(R_{tn}\right)$ to the $\sigma^2_{\hat{n}}\left(S_{tn}\right)$ are calculated. The $\mathrm{cov}(M_{\hat{t}n}, R_{tn})$

can be negative at some conditions, for example, when the depressions correspond to greater $M_{\hat{t}n}$ and more negative $R_{tn}$ values in the discharge periods. This resulted in percentage contributions of $\sigma^2_{\hat{n}}(M_{\hat{t}n})$ and $\sigma^2_{\hat{n}}(R_{tn})$ > 100% and percentage contributions of $2\mathrm{cov}(M_{\hat{t}n}, R_{tn})$ < 0% (Mittelbach and Seneviratne, 2012; Brocca et al., 2014; Rötzer et al., 2015). If $R_{tn}$ is zero at any time or location, there are no interactions between spatial forcing and temporal forcing, $\sigma^2_{\hat{n}}(S_{tn})$ and the spatial trends of SWC are consistent over time. Therefore, $R_{tn}$ is directly responsible for temporal change in the spatial variability of SWC.

If some underlying spatial patterns exist in $R_{tn}$, $R_{tn}$ can be reconstructed by the sum of the product of time-invariant spatial structures (EOFs) and time-dependent coefficients (ECs) using the EOF method. Note that the number of EOF (or EC) series also equals the number of sampling dates.

For estimation of spatially distributed SWC, $R_{tn}$ is estimated by the same method as $Z_{tn}$ using Eq. (3). The $M_{\hat{t}n}$ is estimated with prior measurements by:

$$M_{\hat{t}n} = \frac{1}{m}\sum_{j=1}^{m} S_{tn}, \qquad (9)$$

where $m$ is the number of previous measurement times, and $A_{t\hat{n}}$ is estimated by:

$$A_{t\hat{n}} = S_{t\hat{n}} - M_{\hat{t}\hat{n}}, \qquad (10)$$

where $M_{\hat{t}\hat{n}}$ is the spatial mean of $M_{\hat{t}n}$, and $S_{t\hat{n}}$ is estimated from SWC measurements at the most time-stable location using Eq. (2).

The Pearson correlation coefficient ($R$) is used to explore the linear relationships between various spatial components in the two models (i.e., EOF1 of the $Z_{tn}$ in the SA model, $M_{\hat{t}n}$, and EOF1 of the $R_{tn}$ in the TA model) and environmental factors

263 (i.e., soil, vegetative, and topographical properties). The multiple stepwise regressions
264 are conducted to determine the percentage of variations in the spatial components
265 which the controlling factors explain.

266 **2.3 Validation and performance parameter**

267 The TA model is more complicated than the SA model. In order to evaluate the two
268 models for parsimony, AICc values are calculated (Burnham and Anderson, 2002) as:

269 $$\mathrm{AICc} = 2k + n\ln(RSS/n) + 2k(k+1)/(n-k-1), \qquad (11)$$

270 where $k$ is the number of parameters, $n$ is the sample size, and $RSS$ is the residual sum
271 of squares.

272 Both cross validation and external validation are used to estimate SWC distribution
273 with both models. For the cross validation, an iterative removal of 1 of the 23 dates is
274 made for model development, and the SWC along the transect corresponding to the
275 removed date is estimated iteratively. For the external validation, SWC from 14 dates
276 of the first two years (from July 17, 2007 to May 27, 2009) is used for model
277 development, and the SWC distribution of 9 dates in the second two years (from July
278 21, 2009 to September 29, 2011) is estimated.

279 The Nash-Sutcliffe coefficient of efficiency (NSCE) is used to evaluate the quality
280 of estimation of spatially distributed SWC, which is expressed as:

281 $$\mathrm{NSCE} = 1 - \frac{\sigma_{\varepsilon}^2}{\sigma_{measure}^2}, \qquad (12)$$

282 where $\sigma_{measure}^2$ is the variance of measured SWC, and $\sigma_{\varepsilon}^2$ is the mean squared
283 estimation error. A larger NSCE value implies a better quality of estimation. A paired
284 samples T-test is used to test whether the NSCE values between the TA model and the

285 SA model are statistically significant at $P$<0.05.

286 Many factors may affect the relative performance of spatially distributed SWC
287 estimation between the TA model and the SA model. First, the degree of
288 outperformance of the TA model over the SA model may depend on the amount of
289 $R_{tn}$ variance considered in the TA model. On one hand, the two models are identical
290 if variance of $R_{tn}$ is close to zero or there are negligible interactions between the
291 spatial and temporal components (Fig. 1). On the other hand, if no underlying spatial
292 patterns exist in the $R_{tn}$ or the underlying spatial patterns contributed little to the
293 total variance of the $R_{tn}$, the outperformance will also be very limited. Therefore, the
294 greater the variance of $R_{tn}$ considered in the TA model, the more likely the TA
295 model can outperform the SA model. Second, the way of EOF decomposition may
296 also affect the relative performance. In the SA model, EOF decomposition is
297 performed on lumped time-stable patterns ($M_{\hat{t}n}$) and space-variant temporal anomaly
298 ($R_{tn}$). In the TA model, however, EOF decomposition is made only on the $R_{tn}$. In
299 theory, the two models will be identical if the $M_{\hat{t}n}$ and the first underlying spatial
300 pattern (i.e., EOF1) of the $R_{tn}$ were perfectly correlated. If a nonlinear relationship
301 exists between them, lumping the $M_{\hat{t}n}$ and $R_{tn}$ together, as in the SA model,
302 would weaken the model performance as compared to the TA model. From this aspect,
303 the greater deviation from a linear relationship between the $M_{\hat{t}n}$ and EOF1 of the
304 $R_{tn}$, may lead to a greater outperformance of the TA model over the SA model.
305 Finally, the performances of both models rely on the estimation accuracy of the $\mathrm{EC}_t$
306 which depends on both goodness of fit of the cosine function (i.e., Eq. 4) and

307 estimation accuracy of the $S_{t\hat{n}}$. Because the same $S_{t\hat{n}}$ values are used for the two
308 models, the relative performance of the two models is related to the goodness of fit of
309 Eq. (4).

310 # 3. Results

311 ## 3.1 Components of SWC and their controls

312 ### 3.1.1 Spatial mean ($S_{t\hat{n}}$) and spatial anomaly ($Z_{tn}$)

313 The values of spatial mean ($S_{t\hat{n}}$) in the SA model varied with the seasons (Fig. 3a).
314 In the spring, such as May 2, 2008 and April 20, 2009, snowmelt infiltration resulted
315 in relatively great $S_{t\hat{n}}$ values. In the summer, however, even one month after large
316 rainfall events (such as on July 19, 2008 and June 21, 2009), the high
317 evapotranspiration by fast-growing vegetation resulted in small $S_{t\hat{n}}$ values. The
318 values of $S_{t\hat{n}}$ also varied between inter-annual meteorological conditions. In 2008,
319 there was less precipitation and higher air temperature than in 2010 (Fig. 2). As a
320 result, $S_{t\hat{n}}$ was relatively smaller in 2008 than in 2010.

321 The spatial patterns of spatial anomaly ($Z_{tn}$) were similar to those of original SWC
322 patterns. The values of $Z_{tn}$ in wet periods (e.g., May 13, 2011) were much greater
323 than in dry periods (e.g., August 23, 2008) in depressions (e.g., at a distance of 123
324 and 250 m); at other locations, however, the spatial anomaly was slightly less in wet
325 periods than in dry periods for both soil layers. Moreover, the spatial anomaly in
326 depressions during the wet periods was much greater in the near surface than in the
327 root zone.

When SWCs of all 23 dates were used for model development, only EOF1 was statistically significant (Fig. 4a), which accounted for 84.3% (0–0.2 m) and 86.5% (0–1.0 m) of the variances in the $Z_{tn}$. Correlation analysis indicated that the spatial pattern of EOF1 in the $Z_{tn}$ was identical to the time-stable patterns ($M_{\hat{t}n}$) in the TA model ($R$=1.0). The controls of EOF1 was therefore the same as those of $M_{\hat{t}n}$, and will be discussed later. The relationship between associated EC1 and $S_{t\hat{n}}$ can be fitted well by the cosine function ($R^2$=0.73 at both the near surface and root zone) (Fig. 4b).

### 3.1.2 Time-stable pattern ($M_{\hat{t}n}$), space-invariant temporal anomaly ($A_{t\hat{n}}$), and space-variant temporal anomaly ($R_{tn}$)

Figure 3b displays the three components in the TA model. The first component $M_{\hat{t}n}$ fluctuated along the transect, with high values in depressions and low values on knolls; the $M_{\hat{t}n}$ also had greater spatial variability in the near surface (variance =36.7%$^2$) than in the root zone (variance=19.5%$^2$). For both soil layers, SOC, depth to the $CaCO_3$ layer, sand content, and wetness index are the dominant factors of $M_{\hat{t}n}$; they together explained 74.5% (near surface ) and 75.6% (root zone) of the variances in the $M_{\hat{t}n}$ (Table 1). In addition, the temporal trend of $A_{t\hat{n}}$ was the same as that of $S_{t\hat{n}}$ in the SA model (Fig. 3a) as both represent temporal forcing.

The $R_{tn}$ varied among landscape positions. At a sampling distance of 123 m (in a depression), $R_{tn}$ was negative in dry periods such as August 23, 2008 and positive in wet periods such as May 13, 2011. This was true for all depressions for both the near surface and the root zone. Therefore, topographically lower positions usually

corresponded to more positive $R_{tn}$ during the wet periods and more negative $R_{tn}$ during the dry periods. This implies that topographically lower locations gained more water during recharge and lost more water during discharge due to the interactions of spatial and temporal forcing. Furthermore, the absolute values of $R_{tn}$ were generally greater in the near surface than the root zone, indicating a greater space-variant temporal anomaly for shallower depths.

The SWC variances and associated components (Eq. 8) also varied with time (Fig. 5). Often, wetter conditions corresponded to greater $\sigma^2_{\hat{n}}(S_{tn})$, as further indicated by moderate correlation between $\sigma^2_{\hat{n}}(S_{tn})$ and $S_{t\hat{n}}$ ($R^2$ of 0.51 and 0.38 for the near surface and the root zone, respectively). This was in agreement with others (Gómez-Plaza et al., 2001; Martínez-Fernández and Ceballos, 2003; Hu et al., 2011). Furthermore, there were greater $\sigma^2_{\hat{n}}(S_{tn})$ values at near surface than in the root zone, indicating greater variability of SWC in the near surface.

The time-invariant $\sigma^2_{\hat{n}}(M_{\hat{t}n})$ contributed to the $\sigma^2_{\hat{n}}(S_{tn})$ with percentages ranging from 25 to 795% for the near surface and from 40 to 174% for the root zone (Fig. 5). The $\sigma^2_{\hat{n}}(M_{\hat{t}n})$ exceeded the $\sigma^2_{\hat{n}}(S_{tn})$ mainly under dry conditions, such as July–October in 2008 and 2009. This excess was offset by the $\sigma^2_{\hat{n}}(S_{tn})$ and $2\mathrm{cov}(M_{\hat{t}n}, R_{tn})$, with the latter contributing negatively to the $\sigma^2_{\hat{n}}(S_{tn})$ with mean percentages of 210% for the near surface and 17% for the root zone. In the dry period, the negative contribution from $2\mathrm{cov}(M_{\hat{t}n}, R_{tn})$ was up to 1327% for the near surface and 122% for the root zone. These values are comparable to those in Mittelbach and Seneviratne (2012) and Brocca et al. (2014).

372 The $\sigma_{\hat{n}}^2(R_{tn})$ contributed less than other components (Fig. 5). The percentages of
373 $\sigma_{\hat{n}}^2(R_{tn})$ ranged from 11 to 632% (arithmetic average of 118%) for the near surface
374 and from 6 to 48% (arithmetic average of 19%) for the root zone; $\sigma_{\hat{n}}^2(R_{tn})$ tended to
375 contribute more in drier periods. This indicates that the space-variant temporal
376 anomaly cannot be ignored, particularly in dry conditions. Furthermore, the
377 contribution of $\sigma_{\hat{n}}^2(R_{tn})$ was greater in the near surface than in the root zone,
378 confirming stronger temporal dynamics of soil water at the near surface. Compared
379 with larger scale studies (Mittelbach and Seneviratne, 2012; Brocca et al., 2014),
380 $\sigma_{\hat{n}}^2(R_{tn})$ of the near surface contributed more to $\sigma_{\hat{n}}^2(S_{tn})$, with a mean percentage
381 contribution of 118%, versus 9–68% in the other, larger scale studies. This indicates
382 that interactions between spatial and temporal forcing were stronger, resulting in
383 relatively more intensive temporal dynamics of soil water in our study area than at
384 larger scales.

385 Three significant EOFs of $R_{tn}$ for both soil layers were identified when SWC of
386 all 23 dates were used for model development. The first three EOFs explained 61.1,
387 13.4, and 8.1% respectively, of the total $R_{tn}$ variance for the near surface, and 44.3,
388 20.2, and 12.4%, respectively, of the total $R_{tn}$ variance in the root zone. Therefore,
389 our hypothesis that underlying spatial patterns exist in the $R_{tn}$ was accepted. Due to
390 the negligible contribution of EOF2 and EOF3 to the estimation of spatially
391 distributed SWC, only EOF1 is shown in Fig. 6a. The associated EC1 changed with
392 soil water conditions ($S_{t\hat{n}}$) (Fig. 6b). When SWC was close to average levels, the EC1
393 was close to 0, resulting in negligible $R_{tn}$. This was in accordance with Mittelbach

and Seneviratne (2012) and Brocca et al. (2014), who showed that the spatial variance of the temporal anomaly was the smallest when water contents were close to average levels. The cosine function (Eq. 4) explained a large amount of the variances in EC1 for both soil layers ($R^2$=0.76 at the near surface and 0.88 in the root zone).

The contribution of EOF1 to the space-variant temporal anomaly can be examined through the product of the EOF1 and the associated EC1. The EC1 values tended to be positive during wet periods and negative during dry periods (Fig. 6b); more positive EOF1 values were usually observed at locations with greater $M_{\hat{t}n}$ values (Figs. 3b and 6a). Therefore, the product of EOF1 and EC1 led to greater temporal SWC dynamics at wetter locations of both layers in both the wet and dry periods.

Depth to the $CaCO_3$ layer and SOC had significant, positive correlations with EOF1 for both soil layers ($R$ ranging from 0.76 to 0.88; Table 1). They jointly accounted for 81.6% (near surface) and 81.0% (root zone) of the variances in EOF1. This implies that locations with a greater depth to the $CaCO_3$ layer and SOC, which correspond to wetter locations such as depressions, usually have greater temporal SWC dynamics during both wet and dry periods.

### 3.2 Estimation of spatially distributed SWC

When all 23 datasets were used and only EOF1 was considered, the TA model had an AICc value of 4093 for the near surface and 562 for the root zone, while the corresponding values for the SA model were 6370 and 3460. This indicated that even when penalty to complexity was given, the TA model was better than the SA model. The two models in terms of spatially distributed SWC estimation are compared below.

### 3.2.1 The TA model

The $R_{tn}$ terms and associated EOFs differed slightly with each validation. The number of significant EOFs varied between one (accounting for 60% of the total cases) and three for both soil layers. A paired samples T-test indicated that more EOFs did not result in a significant increase of NSCE in the estimation of spatially distributed SWC for both validation methods, because AICc values increased greatly with the increasing number of parameters resulting from more EOFs (data not shown). This indicates that higher-order EOFs, even if they are statistically significant, are negligible for SWC prediction. Therefore, SWC distribution was estimated with EOF1 only.

Estimated SWCs generally approximated those measured at different soil water conditions during the cross validation (Fig. 7). However, on October 27, 2009, there were unsatisfactory estimates at the 100–140 and 220–225 m locations near the surface. Unsatisfactory NSCE values of -4.05, -1.83, and -3.81 were obtained in the near surface in only three of the 23 dates, which were all in the fall (October 22, 2008, August 27, 2009, and October 27, 2009, respectively). The poor performance obtained with the TA model on those dates was a result of overestimation in depressions, where strong evapotranspiration and deep drainage resulted in a much lower SWC than in the spring. These dates also corresponded to a high percentage of contribution of $\sigma_{\hat{n}}^2(R_{tn})$ to the $\sigma_{\hat{n}}^2(S_{tn})$ (203–439%). For August 23 and September 17 in 2008, which were in dry periods, $\sigma_{\hat{n}}^2(R_{tn})$ of the near surface also contributed highly to the $\sigma_{\hat{n}}^2(S_{tn})$ (580 and 630%). Because a fair amount of $\sigma_{\hat{n}}^2(R_{tn})$ was accounted for

438 with the TA model, the TA model performed satisfactorily (NSCE of 0.43 and 0.60).
439 For the remaining 20 dates, the resulting NSCE value ranged from 0.38 to 0.90 in the
440 near surface and from 0.65 to 0.96 in the root zone (Fig. 8). This suggests that the TA
441 model was generally satisfactory, with better performance in the root zone than in the
442 near surface.

443 During the external validation, the TA model resulted in SWC estimations with
444 NSCE values ranging from 0.61 to 0.85 near the surface and from 0.32 to 0.92 in the
445 root zone, with exception of two days (August 27, 2009 and October 27, 2009 with
446 NSCE values of -2.63 and -5.12, respectively) at 0–0.2 m (Fig. 8). This suggested that
447 the TA model performed well in estimating spatially distributed SWC patterns except
448 on August 27, 2009 and October 27, 2009 at 0–0.2 m. The estimation in the root zone
449 was also generally better than in the near surface.

450 **3.2.2 Comparison with the SA model**

451 One significant EOF of $Z_{tn}$ was identified for both soil layers, irrespective of the
452 validation method. The SA model with only EOF1 produced reasonable SWC
453 estimations for both validations in all dates in the root zone and in every date except
454 five dates (August 23, 2008, September 17, 2008, October 22, 2008, August 27, 2009,
455 and October 27, 2009) in the near surface (Fig. 8). Similarly, when more EOFs were
456 included, NSCE values did not increase significantly (data not shown) and
457 consequently, estimation of spatially distributed SWC was not improved. This was
458 because EOF2 and EOF3 together explained a very limited (<10%) amount of
459 variability of $Z_{tn}$ and thus had low predictive power in terms of variance.

The difference in NSCE values between the TA and SA models for both validations are presented in Fig. 9. Generally, the difference decreased as $A_{t\hat{n}}$ increased, and then slightly increased with a further increase in $A_{t\hat{n}}$. A paired samples T-test indicated that the NSCE values of the TA model were significantly ($P$<0.05) greater than those of the SA model for both soil layers, irrespective of validation methods. This indicates that the TA model outperformed the SA model, particularly in dry conditions. This was because when the soil was dry, there was a high contribution of $\sigma_{\hat{n}}^2(R_{tn})$, and thus strong variability in the space-variant temporal anomaly.

### 3.3 Further application at other two sites with different scales

#### 3.3.1 A hillslope in the Chinese Loess Plateau

Along a hillslope of 100 m in length in the Chinese Loess Plateau, SWC of 0–0.06 m was measured 136 times from June 25, 2007 to August 30, 2008 by a Delta-T Devices Theta probe (ML2x) at 51 locations (Hu et al., 2011). The hillslope was covered by *Stipa bungeana* Trin. and *Medicago sativa* L. in sandy loam and silt loam soils. On average, the $\sigma_{\hat{n}}^2(M_{\hat{t}n})$, $\sigma_{\hat{n}}^2(R_{tn})$, and $2\mathrm{cov}(M_{\hat{t}n}, R_{tn})$ contributed 53, 74 and -27% to the $\sigma_{\hat{n}}^2(S_{tn})$, indicating that both time-stable pattern and temporal anomalies were the main contributors to the $\sigma_{\hat{n}}^2(S_{tn})$. The EOF analysis showed that only the EOF1 was statistically significant for both the $R_{tn}$ and $Z_{tn}$, and the EOF1 explained 23% and 47% of the total variances of $R_{tn}$ and $Z_{tn}$, respectively. This illustrated that underlying spatial patterns exist in the $R_{tn}$ on the hillslope. Cross validation was used to estimate the spatially distributed SWC along the hillslope. The results showed that the NSCE varied from -4.25 to 0.83 (TA model) and from -4.30 to

0.81 (SA model), with a mean value of 0.25 and 0.18, respectively. A paired samples T-test showed that the NSCE values for the TA model were significantly ($P$<0.05) greater than those for the SA model, indicating that the TA model outperformed the SA model. As Fig. 10a shows, the outperformance was greater when SWC deviated from intermediate conditions, especially for dry conditions, which was similar to the Canadian site.

### 3.3.2 The GENCAI network in Italy

In the GENCAI network (~250 km²) in Italy, SWC of 0–0.15 m was measured by a TDR probe at 46 locations, 34 times from February to December in 2009 (Brocca et al., 2012, 2013). The GENCAI area was dominated by grassland with a flat topography, in silty clay soils. The $\sigma_{\hat{n}}^2\left(M_{\hat{t}n}\right)$, $\sigma_{\hat{n}}^2\left(R_{tn}\right)$, and $2\mathrm{cov}(M_{\hat{t}n}, R_{tn})$ contributed 38, 68, and -7% to the $\sigma_{\hat{n}}^2\left(S_{tn}\right)$ (Brocca et al., 2014), indicating the dominant contribution of temporal anomalies on SWC variability. The first three EOFs of the $R_{tn}$ explained 19, 16, and 8% of the total $\sigma_{\hat{n}}^2\left(R_{tn}\right)$, and no EOFs were statistically significant, indicating that no underlying spatial patterns exist in the $R_{tn}$. The EOF1 of the $Z_{tn}$ was significant and accounted for 37% of the variances in the $Z_{tn}$. Although the EOF1 of the $R_{tn}$ was not significant, it was considered in the TA model for estimating spatially distributed SWC. The cross validation indicates that the NSCE varied from -0.79 to 0.50 (TA model) and from -0.87 to 0.56 (SA model), with mean values of 0.09 and 0.08, respectively. The SWC estimation based on these two models was not satisfactory except for a few days. As Fig. 10b shows, the differences in NSCE values between the two models were scattered around 0. A paired samples

T-test showed that the NSCE values between the TA model and the SA model were not significant ($P$<0.05), indicating no differences in estimating spatially distributed SWC between these two models.

# 4 Discussion

## 4.1 Controls of the $M_{\hat{t}n}$ and $R_{tn}$

The $R_{tn}$ played an important role in the temporal change in spatial patterns of the SWC. The underlying spatial patterns and physical meaning in the $R_{tn}$ were examined in our study for the first time. Although three significant EOFs of the $R_{tn}$ existed in some cases, only EOF1 rather than higher-order EOFs of the $R_{tn}$ should be considered for the spatially distributed SWC estimation. Among many factors influencing the EOF1 of the $R_{tn}$, depth to the $CaCO_3$ layer followed by the SOC, were the most important factors. Depressions have deeper $CaCO_3$ layers than knolls, and the shallow $CaCO_3$ layer on knolls limited water infiltration during rainfall or snowmelt, resulting in less water recharge on knolls than in depressions. The depth to $CaCO_3$ layer and SOC were negatively correlated with elevation ($R$=-0.54, $P$<0.01). Therefore, the influence of depth to $CaCO_3$ layer and SOC partially reflected the role of topography in driving snowmelt runoff along slopes in the spring, which contributes to increasing water recharge in depressions. Locations with greater SOC usually corresponded to vegetation with a larger leaf area index ($R$=0.23, $P$<0.05), which would also result in higher evapotranspiration and more water loss during discharge periods.

As Table 1 shows, both the depth to the $CaCO_3$ layer and SOC controlled the $M_{\hat{t}n}$. This was because deeper $CaCO_3$ layers and higher SOC were observed in depressions where soils were usually wetter in most of the year because of the snowmelt runoff in the spring and rainfall runoff in the summer and autumn (van der Kamp et al., 2003). Therefore, the roles of soil and topography were two-fold: On one hand, they were highly correlated with the time-stable patterns and thus the time stability of SWC (Gómez-Plaza et al., 2000; Mohanty and Skaggs, 2001; Grant et al., 2004); On the other hand, soil and topography, interplaying with temporal forcing, triggered local-specific soil water change and destroyed time stability of SWC. Their roles in protecting time stability persisted, but their roles in destroying time stability varied with time. Greater $\sigma_{\hat{n}}^2(R_{tn})$ implies greater contribution of these factors in soil water dynamics, resulting in less time stability of SWC.

### 4.2 Model performance for spatially distributed SWC estimation

The outperformance of the TA model for estimating spatial SWC at the Canadian site and Chinese site can be partly explained by the high contribution percentages (average of 19–118%) of the $\sigma_{\hat{n}}^2(R_{tn})$ to the total variance. When SWC is close to average levels, $R_{tn}$ is also close to zero, resulting in negligible variance contribution from $R_{tn}$ to the total variance. In this case, the soil water patterns are stable, the SA model performs well, and there will be little differences between these two models. As is well known, the spatial patterns in soil water content are inherently time unstable. For example, when evapotranspiration becomes the dominant process at the small watershed scale, more water will be lost in depressions due to the denser

547 vegetation than on knolls (Millar, 1971; Biswas et al., 2012), effectively diminishing
548 the spatial patterns and increasing temporal instability. In this case, the $\sigma_{\hat{n}}^2(R_{tn})$
549 contributes more to the total variance (e.g., high up to 632%) and the TA model may
550 outperform the SA model. This explained why the outperformance of the TA model
551 was more obvious in the dry conditions. For the GENCAI network in Italy, although
552 the $\sigma_{\hat{n}}^2(R_{tn})$ contributed 68% of the total variance, the performance of the TA model
553 was identical to the SA model. This was because there were no underlying spatial
554 patterns in the $R_{tn}$. Similarly, because the first underlying spatial pattern (i.e., EOF1)
555 explained greater percentages of the $\sigma_{\hat{n}}^2(R_{tn})$ at the Canadian site (44–61%) than the
556 Chinese site (23%), the outperformance of the TA model over the SA model was more
557 obvious at the former site (Fig. 9 and 10a). Therefore, the TA model is advantageous
558 only if the contribution of $\sigma_{\hat{n}}^2(R_{tn})$ to the total variance is substantial and underlying
559 spatial patterns exist in the $R_{tn}$.

560 The existence of underlying spatial patterns in the $R_{tn}$ is related to the controlling
561 factors, which may be scale-specific. At small scales, “static” factors such as the depth
562 to the $CaCO_3$ layer and SOC at the Canadian site may affect not only the time-stable
563 patterns but also the $R_{tn}$. The persistent influence of “static” factors on the $R_{tn}$
564 resulted in significant underlying spatial patterns in the $R_{tn}$. Thus, the TA model
565 outperformed the SA model at the small scales. At large scales such as the basin scale
566 or greater, time-stable patterns may be controlled by, in addition to soil and
567 topography (Mittelbach and Seneviratne, 2012), the climate gradient (Sherratt and
568 Wheater, 1984); at those scales, $R_{tn}$ is more likely to be controlled by the

meteorological anomaly (i.e., spatially random variation) (Walsh and Mostek, 1980), and the effects of soil and topography may be reduced. Consequently, spatial patterns in the $R_{tn}$ may be weakened and the TA model may have no advantages over the SA model such as for the Italian site.

The $M_{\hat{t}n}$ and the underlying spatial patterns (EOF1) in the $R_{tn}$ were controlled by the same spatial forcing (e.g., depth to $CaCO_3$ layer and SOC) at the Canadian site (Table 1), and they were correlated with an $R^2$ of 0.83 for the near surface and 0.42 for the root zone. Although the relationships between $M_{\hat{t}n}$ and $R_{tn}$ were strong, they were not strictly linear, suggesting that $M_{\hat{t}n}$ and $R_{tn}$ were affected differently by these factors. Therefore, the nonlinear relationship between $M_{\hat{t}n}$ and $R_{tn}$ partially contributed to the outperformance of the TA model over the SA model.

The relationship between the $S_{t\hat{n}}$ and EC1 was better fitted by the cosine function in the TA model than the SA model (Figs. 4b and 6b), with $R^2$ of 0.76 versus 0.73 in the near surface and 0.88 versus 0.73 in the root zone. The reduced scatter in the $S_{t\hat{n}}$ and EC1 relationship for the TA model may also partly explain the outperformance of the TA model over the SA model.

Therefore, the outperformance of the TA model over the SA model depends on counterbalance among the variance of $R_{tn}$ explained in the TA model, the linear correlation between the $M_{\hat{t}n}$ and EOF1 of the $R_{tn}$, and the goodness of fit for the $S_{t\hat{n}}$ and EC1 relationship. For example, the variance of EOF1 in the $R_{tn}$ for the near surface (i.e., $264\%^2$) was much greater than that for the root zone (i.e., $43\%^2$). However, $M_{\hat{t}n}$ and underlying spatial patterns (EOF1) in the $R_{tn}$ in the root zone

591 deviated more from a linear relationship, and the reduced scatter in the $S_{t\hat{n}}$ and EC1
592 relationship in the TA model was more obviously in the root zone than in the near
593 surface. As a result, the outperformance of the TA model was comparable between the
594 near surface and root zone at the Canadian site (Fig. 9).

595 In the real world, the relations between the $M_{\hat{t}n}$ and underlying spatial patterns in
596 the $R_{tn}$ may rarely be perfectly linear. Therefore, when underlying spatial patterns
597 exist in the $R_{tn}$ and the $R_{tn}$ has substantial variances, the TA model is preferable
598 to the SA model for the estimation of spatially distributed SWC. Because the TA
599 model was not worse than the SA model for the whole range of SWC, the TA model is
600 suggested for the estimation of spatially distributed SWC at different soil water
601 conditions.

602 Previous studies on SWC decomposition mainly focus on near surface layers
603 (Jawson and Niemann, 2007; Perry and Niemann, 2007, 2008; Joshi and Mohanty,
604 2010; Korres et al., 2010; Busch et al., 2012). This study decomposed spatiotemporal
605 SWC using the TA model for both the near surface and the root zone. The results
606 showed that the estimation of spatially distributed SWC at small watershed scales was
607 improved by the TA method that considers the $R_{tn}$. Because of the stronger time
608 stability of SWC in deeper soil layers (Biswas and Si, 2011), SWC evaluation in
609 thicker soil layers was more accurate than in shallow soil layers. This is particularly
610 important because SWC data for deeper soil layers in a watershed is more difficult to
611 collect than that of surface soil.

612 # 5 Conclusions

613 The TA model was used to decompose spatiotemporal SWC into time-stable
614 patterns $M_{\hat{t}n}$, space-invariant temporal anomaly $A_{t\hat{n}}$, and space-variant temporal
615 anomaly $R_{tn}$. This study indicated that underlying spatial patterns may exist in the
616 $R_{tn}$ at small scales (e.g., small watersheds and hillslope) but may not exist at large
617 scales such as the GENCAI network (~250 km²) in Italy. This was because the $R_{tn}$
618 at small scales was driven by "static" factors such as depth to the $CaCO_3$ layer and
619 SOC at the Canadian site, while the $R_{tn}$ at large scales may be dominated by
620 "dynamic" factors such as meteorological anomaly. Compared to the SA model,
621 estimation of spatially distributed SWC was improved with the TA model at small
622 watershed scales. This was because the TA model considered a fair amount of spatial
623 variance in the $R_{tn}$, which was ignored in the SA model. Furthermore, the improved
624 performance was observed mainly when there was less or more soil water than the
625 average level, especially in drier conditions due to the high $\sigma_{\hat{n}}^2(R_{tn})$ value.

626 This study showed that outperformance of the TA model over the SA model is
627 possible when $\sigma_{\hat{n}}^2(R_{tn})$ contributes substantial variance to the total variance of SWC,
628 and significant spatial patterns (or EOFs) exist in the $R_{tn}$. Further application of the
629 TA model for the estimation of spatially distributed SWC at different scales and
630 hydrological backgrounds is recommended. If the TA model parameters (i.e., $M_{\hat{t}n}$,
631 EOF1 of the $R_{tn}$, and relationship between EC and $S_{t\hat{n}}$) are obtained from historical
632 SWC datasets, a detailed spatially distributed SWC of near surface soil at watershed
633 scales can be constructed from remote sensed SWC. Note that both models rely on

previous SWC measurements for model parameters. Therefore, ~~the future study~~ should be directed to estimate spatially distributed SWC in un-gauged watersheds based on the estimation of the model parameters using pedotransfer functions. Since the TA model needs one more spatial parameter (i.e., $M_{\hat{t}n}$) than the SA model, the advantage of the TA model may be weakened. Nevertheless, the TA model may be preferred if it estimates spatial SWC much better than the SA model such as under dry conditions. The codes for decomposing SWC with the SA and TA models and related EOF analysis were written in Matlab and are freely available from the authors upon request.

## Acknowledgements

This project was funded by the Natural Sciences and Engineering Research Council (NSERC) of Canada. We thank Dr. Asim Biswas, Dr. Henry Wai Chau, Mr. Trent Pernitsky, and Mr. Eric Neil for their help in data collection. We thank the anonymous reviewers and the Editor for their constructive comments.

## References

Biswas, A., Chau, H. W., Bedard-Haughn, A., and Si, B. C.: Factors controlling soil water storage in the Hummocky landscape of the Prairie Pothole region of North America, Can. J. Soil Sci., 92, 649–663, doi: 10.4141/CJSS2011-045, 2012.

Biswas, A. and Si, B. C.: Scales and locations of time stability of soil water storage in a hummocky landscape, J. Hydrol., 408, 100–112, doi: 10.1016/j.jhydrol.2011.07.027,

654 2011.
655 Blöschl, G., Komma, J., and Hasenauer, S.: Hydrological downscaling of soil
656 moisture, Final report to the H-SAF (Hydrology Satellite Application Facility) via the
657 Austrian Central Institute for Meteorology and Geodynamics (ZAMG), Vienna
658 University of Technology, A-1040 Vienna, Austria, 2009.
659 Brocca, L., Melone, F., Moramarco, T., and Morbidelli, R.: Soil moisture temporal
660 stability over experimental areas in Central Italy, Geoderma, 148, 364–374, doi:
661 10.1016/j.geoderma.2008.11.004, 2009.
662 Brocca, L., Tullo, T., Melone, F., Moramarco, T., and Morbidelli, R.: Catchment scale
663 soil moisture spatial-temporal variability, J. Hydrol., 422-423, 63–75,
664 doi:10.1016/j.jhydrol.2011.12.039, 2012.
665 Brocca, L., Zucco, G., Mittelbach, H., Moramarco, T., and Seneviratne, S. I.: Absolute
666 versus temporal anomaly and percent of saturation soil moisture spatial variability for
667 six networks worldwide, Water Resour. Res., 50, 5560–5576, doi:
668 10.1002/2014WR015684, 2014.
669 Brocca, L., Zucco, G., Moramarco, T., and Morbidelli, R.: Developing and testing a
670 long-term soil moisture dataset at the catchment scale, J. Hydrol., 490, 144–151, doi:
671 10.1016/j.jhydrol.2013.03.029, 2013.
672 Burnham, K. P. and Anderson, D. R.: Model selection and multimodel inference: A
673 practical information-theoretic approach (2nd ed.), Springer-Verlag, New York, 2002.
674 Busch, F. A., Niemann, J. D., and Coleman, M.: Evaluation of an empirical
675 orthogonal function-based method to downscale soil moisture patterns based on

topographical attributes, Hydrol. Process., 26, 2696–2709, doi: 10.1002/hyp.8363, 2012.

Champagne, C., Berg, A. A., McNairn, H., Drewitt, G., and Huffman, T.: Evaluation of soil moisture extremes for agricultural productivity in the Canadian prairies, Agric. For. Meteorol., 165, 1–11, doi: 10.1016/j.agrformet.2012.06.003, 2012.

Famiglietti, J. S., Rudnicki, J. W., and Rodell, M.: Variability in surface moisture content along a hillslope transect: Rattlesnake Hill, Texas, J. Hydrol., 210, 259–281, doi: 10.1016/S0022-1694(98)00187-5, 1998.

Gómez-Plaza, A., Alvarez-Rogel, J., Albaladejo, J., and Castillo, V. M.: Spatial patterns and temporal stability of soil moisture across a range of scales in a semi-arid environment, Hydrol. Process., 14, 1261–1277, doi: 10.1002/(SICI)1099-1085(200005)14:7<1261::AID-HYP40>3.0.CO;2-D, 2000.

Gómez-Plaza, A., Martínez-Mena, M., Albaladejo, J., and Castillo, V. M.: Factors regulating spatial distribution of soil water content in small semiarid catchments, J. Hydrol., 253, 211–226, doi: 10.1016/S0022-1694(01)00483-8, 2001.

Grant, L., Seyfried, M., and McNamara, J.: Spatial variation and temporal stability of soil water in a snow-dominated, mountain catchment, Hydrol. Process., 18, 3493–3511, doi: 10.1002/hyp.5789, 2004.

Grayson, R. B. and Western, A. W.: Towards areal estimation of soil water content from point measurements: Time and space stability of mean response, J. Hydrol., 207, 68–82, doi: 10.1016/S0022-1694(98)00096-1, 1998.

Hu, W., Shao, M. A., Han, F. P., and Reichardt, K.: Spatio-temporal variability

698 behavior of land surface soil water content in shrub- and grass-land, Geoderma, 162,
699 260–272, doi: 10.1016/j.geoderma.2011.02.008, 2011.
700 Hu, W., Shao, M. A., and Reichardt, K.: Using a new criterion to identify sites for
701 mean soil water storage evaluation, Soil Sci. Soc. Am. J., 74, 762–773, doi:
702 10.2136/sssaj2009.0235, 2010.
703 Hu, W., Tallon, L. K., and Si, B. C.: Evaluation of time stability indices for soil water
704 storage upscaling, J. Hydrol., 475, 229–241, doi: 10.1016/j.jhydrol.2012.09.050,
705 2012.
706 Jawson, S. D. and Niemann, J. D.: Spatial patterns from EOF analysis of soil moisture
707 at a large scale and their dependence on soil, land-use, and topographic properties,
708 Adv. Water Resour., 30, 366–381, doi:10.1016/j.advwatres.2006.05.006, 2007.
709 Jia, Y. H. and Shao, M. A.: Temporal stability of soil water storage under four types of
710 revegetation on the northern Loess Plateau of China, Agric. Water Manage., 117,
711 33–42, doi: 10.1016/j.agwat.2012.10.013, 2013.
712 Johnson, R. A. and Wichern, D. W.: Applied multivariate statistical analysis, Prentice
713 Hall, Upper Saddle River, New Jersey, 2002.
714 Joshi, C. and Mohanty, B. P.: Physical controls of near-surface soil moisture across
715 varying spatial scales in an agricultural landscape during SMEX02, Water Resour.
716 Res., 46, doi: 10.1029/2010WR009152, 2010.
717 Korres, W., Koyama, C. N., Fiener, P., and Schneider, K.: Analysis of surface soil
718 moisture patterns in agricultural landscapes using Empirical Orthogonal Functions,
719 Hydrol. Earth Syst. Sci., 14, 751–764, doi: 10.5194/hess-14-751-2010, 2010.

720 Martínez-Fernández, J. and Ceballos, A.: Temporal stability of soil moisture in a
721 large-field experiment in Spain, Soil Sci. Soc. Am. J., 67, 1647–1656, 2003.
722 Millar, J. B.: Shoreline-area ratios as a factor in rate of water loss from small sloughs,
723 J. Hydrol., 14, 259–284, doi: 10.1016/0022-1694(71)90038-2, 1971.
724 Mittelbach, H. and Seneviratne, I.: A new perspective on the spatio-temporal
725 variability of soil moisture: Temporal dynamics versus time-invariant contributions,
726 Hydrol. Earth Syst. Sci., 16, 2169–2179, doi: 10.5194/hess-16-2169-2012, 2012.
727 Mohanty, B. P. and Skaggs, T. H.: Spatio-temporal evolution and time–stable
728 characteristics of soil moisture within remote sensing footprints with varying soil
729 slope and vegetation, Adv. Water Resour., 24, 1051–1067, doi:
730 10.1016/S0309-1708(01)00034-3, 2001.
731 Peel, M. C., Finlayson, B. L., and McMahon, T. A.: Updated world map of the
732 Köppen-Geiger climate classification, Hydrol. Earth Syst. Sci., 11, 1633–1644,
733 doi:10.5194/hess-11-1633-2007, 2007.
734 Perry, M. A. and Niemann J. D.: Analysis and estimation of soil moisture at the
735 catchment scale using EOFs, J. Hydrol., 334, 388–404, doi:
736 10.1016/j.jhydrol.2006.10.014, 2007.
737 Perry, M. A. and Niemann J. D.: Generation of soil moisture patterns at the catchment
738 scale by EOF interpolation, Hydrol. Earth Syst. Sci., 12, 39–53,
739 doi:10.5194/hess-12-39-2008, 2008.
740 Robinson, D. A., Campbell, C. S., Hopmans, J. W., Hornbuckle, B. K., Jones, S. B.,
741 Knight, R., Ogden, F., Selker, J., and Wendroth, O.: Soil moisture measurement for

742 ecological and hydrological watershed-scale observatories: A review, Vadose Zone J.,
743 7, 358–389, doi: 10.2136/vzj2007.0143, 2008.
744 Rötzer, K., Montzka, C., and Vereecken, H.: Spatio-temporal variability of global soil
745 moisture products, J. Hydrol., 522, 187–202, doi: 10.1016/j.jhydrol.2014.12.038,
746 2015.
747 She, D. L., Liu, D. D., Peng, S. Z., and Shao, M. A.: Multiscale influences of soil
748 properties on soil water content distribution in a watershed on the Chinese Loess
749 Plateau, Soil Sci., 178, 530–539, doi: 10.1016/j.jhydrol.2014.08.034, 2013a.
750 She, D. L., Xia, Y. Q., Shao, M. A., Peng, S. Z., and Yu, S. E.: Transpiration and
751 canopy conductance of Caragana Korshinskii trees in response to soil moisture in
752 sand land of China, Agrofor. Syst., 87, 667–678, doi: 10.1007/s10457-012-9587-4,
753 2013b.
754 Sherratt, D. J. and Wheater, H. S.: The use of surface-resistance soil-moisture
755 relationships in soil-water budget models, Agric. For. Meteorol., 31, 143–157, doi:
756 10.1016/0168-1923(84)90016-9, 1984.
757 Soil Survey Staff: Soil Taxonomy, 11th edition, USDA National Resources
758 Conservation Services, Washington DC, 2010.
759 Starr, G. C.: Assessing temporal stability and spatial variability of soil water patterns
760 with implications for precision water management, Agric. Water Manage., 72,
761 223–243, doi: 10.1016/j.agwat.2004.09.020, 2005.
762 Vachaud, G., De Silans, A. P., Balabanis, P., and Vauclin, M.: Temporal stability of
763 spatially measured soil water probability density function, Soil Sci. Soc. Am. J., 49,

764 822–828, 1985.

765 van der Kamp, G., Hayashi, M., and Gallen, D.: Comparing the hydrology of grassed
766 and cultivated catchments in the semi-arid Canadian prairies, Hydrol. Process., 17,
767 559–575, doi: 10.1002/hyp.1157, 2003.

768 Vanderlinden, K., Vereecken, H., Hardelauf, H., Herbst, M., Martinez, G., Cosh, M.
769 H., and Pachepsky, Y. A.: Temporal stability of soil water contents: A review of data
770 and analyses, Vadose Zone J., 11, 4, doi: 10.2136/vzj2011.0178, 2012.

771 Vereecken, H., Kamai, T., Harter, T., Kasteel, R., Hopmans, J., and Vanderborght, J.:
772 Explaining soil moisture variability as a function of mean soil moisture: A stochastic
773 unsaturated flow perspective, Geophys. Res. Lett., 34, L22402, doi:
774 10.1029/2007GL031813, 2007.

775 Venkatesh, B., Nandagiri, L., Purandara, B. K., and Reddy, V. B.: Modelling soil
776 moisture under different land covers in a sub-humid environment of Western Ghats,
777 India, J. Earth Syst. Sci., 120, 387–398, 2011.

778 Walsh, J. E. and Mostek, A.: A quantitative-analysis of meteorological anomaly
779 patterns over the United-States, 1900–1977, Mon. Weather Rev., 108, 615–630, doi:
780 10.1175/1520-0493(1980)108<0615:AQAOMA>2.0.CO;2, 1980.

781 Wang, Y. Q., Shao, M. A., Liu. Z. P., and Warrington, D. N.: Regional spatial pattern
782 of deep soil water content and its influencing factors, Hydrolog. Sci. J., 57, 265–281,
783 doi: 10.1080/02626667.2011.644243, 2012.

784 Ward, P. R., Flower, K. C., Cordingley, N., Weeks, C., and Micin, S. F.: Soil water
785 balance with cover crops and conservation agriculture in a Mediterranean climate,

786 Field Crop. Res., 132, 33–39, doi: 10.1016/j.fcr.2011.10.017, 2012.

787 Zhao, Y., Peth, S., Wang, X. Y., Lin, H., and Horn, R.: Controls of surface soil

788 moisture spatial patterns and their temporal stability in a semi-arid steppe, Hydrol.

789 Process., 24, 2507–2519, doi: 10.1002/hyp.7665, 2010.

## Figure captions

**Figure 1.** Decomposition of spatiotemporal soil water content (SWC) in different models.

**Figure 2.** Daily mean air temperature and precipitation during the study period.

**Figure 3.** Components of soil water content in (a) the SA model (spatial mean soil water content $S_{t\hat{n}}$ and spatial anomaly $Z_{tn}$) and in (b) the TA model (time-stable pattern $M_{\hat{t}n}$, space-invariant temporal anomaly $A_{t\hat{n}}$, and space-variant temporal anomaly $R_{tn}$) for 0–0.2 and 0–1.0 m. Also shown is the elevation.

**Figure 4.** (a) The EOF1 of the spatial anomaly $Z_{tn}$ and (b) relationships of associated EC1 versus spatial mean soil water content $Z_{tn}$ fitted by the cosine function (Eq. 4).

**Figure 5.** Spatial variances of different components in Eq. (8) expressed in $\%^2$ (upper panel) and as percentage (lower panel) for (a) 0–0.2 and (b) 0–1.0 m. Spatial mean soil water content $S_{t\hat{n}}$ on each measurement day is also shown.

**Figure 6.** (a) The EOF1 of the space-variant temporal anomaly $R_{tn}$ and (b) relationships of associated EC1 versus spatial mean soil water content $S_{t\hat{n}}$ fitted by the cosine function (Eq. 4).

**Figure 7.** Estimated soil water content (SWC) versus measured SWC for three dates at different soil water conditions (August 23, 2008, October 27, 2009, and May 13, 2011 are associated with relatively dry, medium, and wet days, respectively) using the TA model for (a) 0–0.2 and (b) 0–1.0 m.

**Figure 8.** The Nash-Sutcliffe coefficient of efficiency (NSCE) of soil water content

812 estimation using the TA and SA models for (a) 0–0.2 and (b) 0–1.0 m for both cross
813 validation (CV) and external validation (EV). At 0–0.2 m, negative Nash-Sutcliffe
814 coefficient of efficiency values for three dates (October 22, 2008, August 27, 2009,
815 and October 27, 2009) are not shown. Spatial mean soil water content $S_{t\hat{n}}$ on each
816 measurement day is also shown.

817 **Figure 9.** Difference between the Nash-Sutcliffe coefficient of efficiency (NSCE) of
818 soil water content estimation by both cross validation (CV) and external validation
819 (EV) using the TA and SA models as a function of space-invariant temporal anomaly
820 $A_{t\hat{n}}$ for (a) 0–0.2 and (b) 0–1.0 m.

821 **Figure 10.** Difference between the Nash-Sutcliffe coefficient of efficiency (NSCE) of
822 soil water content evaluation by the cross validation using the TA and SA models as a
823 function of space-invariant temporal anomaly $A_{t\hat{n}}$ for (a) 0–0.06 m of the Chinese
824 Loess Plateau hillslope and (b) 0–0.15 m of the GENCAI network in Italy.

**Table 1.** Pearson correlation coefficients between time-stable pattern $M_{\hat{t}n}$, EOF1 of space-variant temporal anomaly $R_{tn}$ and various properties.

| | 0–0.2 m | | 0–1.0 m | |
|---|---|---|---|---|
| | $M_{\hat{t}n}$ | EOF1 | $M_{\hat{t}n}$ | EOF1 |
| Sand content | -0.52** | -0.36** | -0.66** | -0.26** |
| Silt content | 0.29** | 0.14 | 0.40** | 0.06 |
| Clay content | 0.43** | 0.38** | 0.51** | 0.33** |
| Organic carbon | 0.78** | 0.83** | 0.73** | 0.76** |
| Wetness index | 0.64** | 0.59** | 0.68** | 0.56** |
| Depth to $CaCO_3$ layer | 0.77** | 0.84** | 0.65** | 0.88** |
| A horizon depth | 0.51** | 0.62** | 0.44** | 0.65** |
| C horizon depth | 0.66** | 0.69** | 0.58** | 0.76** |
| Bulk density | -0.58** | -0.67** | -0.46** | -0.62** |
| Elevation | -0.24** | -0.28** | -0.24** | -0.32** |
| Specific contributing area | 0.20* | 0.24** | 0.24** | 0.23** |
| Convergence index | -0.58** | -0.56** | -0.55** | -0.58** |
| Curvature | -0.10 | -0.08 | -0.19* | -0.16 |
| Cos(aspect) | 0.05 | 0.04 | 0.08 | 0.05 |
| Gradient | -0.12 | -0.09 | -0.21* | -0.02 |
| Slope | -0.51** | -0.48** | -0.56** | -0.44** |
| Upslope length | 0.19* | 0.21* | 0.21* | 0.25** |
| Solar radiation | -0.07 | 0.03 | -0.11 | 0.08 |
| Flow connectivity | 0.45** | 0.43** | 0.49** | 0.49** |
| Leaf area index | -0.07 | 0.06 | -0.10 | -0.14 |
| Variance explained[1] | 74.5% | 81.6% | 75.6% | 81.0% |

[1]percent of variance explained by the controlling factors obtained by the multiple stepwise regressions.
*Significant at $P<0.05$; ** Significant at $P<0.01$.

**Table A1.** Notations.

| | |
|---|---|
| $M_{\hat{t}\hat{n}}$ | spatial mean of $M_{\hat{t}n}$ |
| $R_{tn}$ | space-variant temporal anomaly of SWC at location *n* and time *t* |
| $A_{t\hat{n}}$ | space-invariant temporal anomaly of SWC at time *t* |
| $Z_{tn}$ | spatial anomaly of SWC at location *n* and time *t* |
| $S_{t\hat{n}}$ | spatial mean SWC at time *t* |
| $\sigma^2_{\hat{n}}$ | spatial variance |
| $A_{tn}$ | temporal anomaly of SWC at location *n* and time *t* |
| $\delta_{\hat{t}n}$ | temporal mean relative difference of SWC at location *n* |
| COV | spatial covariance |
| $S_{tn}$ | SWC at location *n* and time *t* |
| $M_{\hat{t}n}$ | time-stable pattern of SWC |
| ECs | temporally-varying coefficients of $R_{tn}$ (or $Z_{tn}$) |
| EOFs | time-invariant spatial structures of $R_{tn}$ (or $Z_{tn}$) |
| NSCE | Nash-Sutcliffe coefficient of efficiency |
| *R* | Pearson correlation coefficient |
| SWC | soil water content |

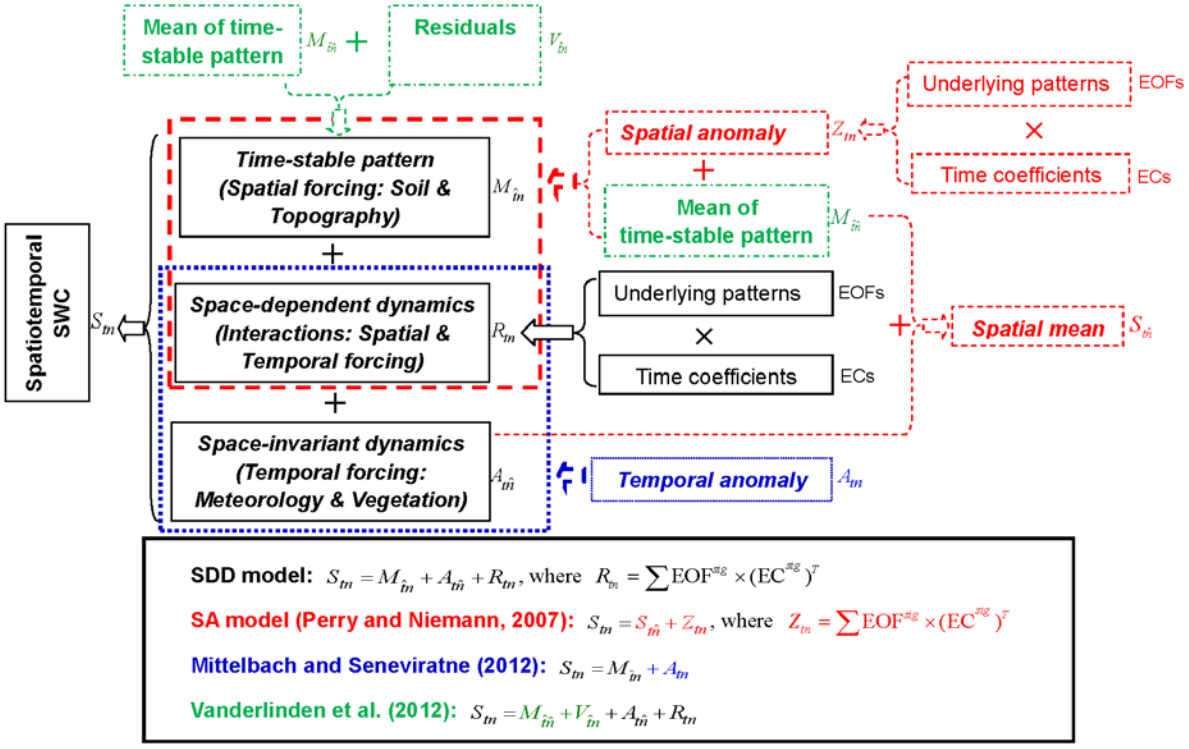


Fig. 1. Decomposition of spatiotemporal soil water content (SWC) in different models.

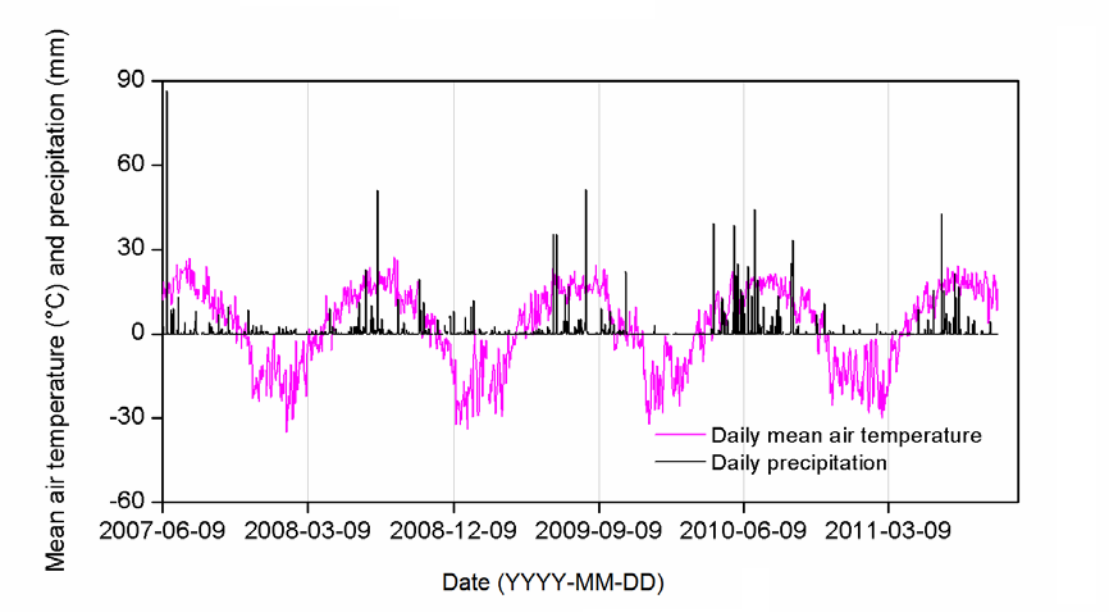


Fig. 2. Daily mean air temperature and precipitation during the study period.

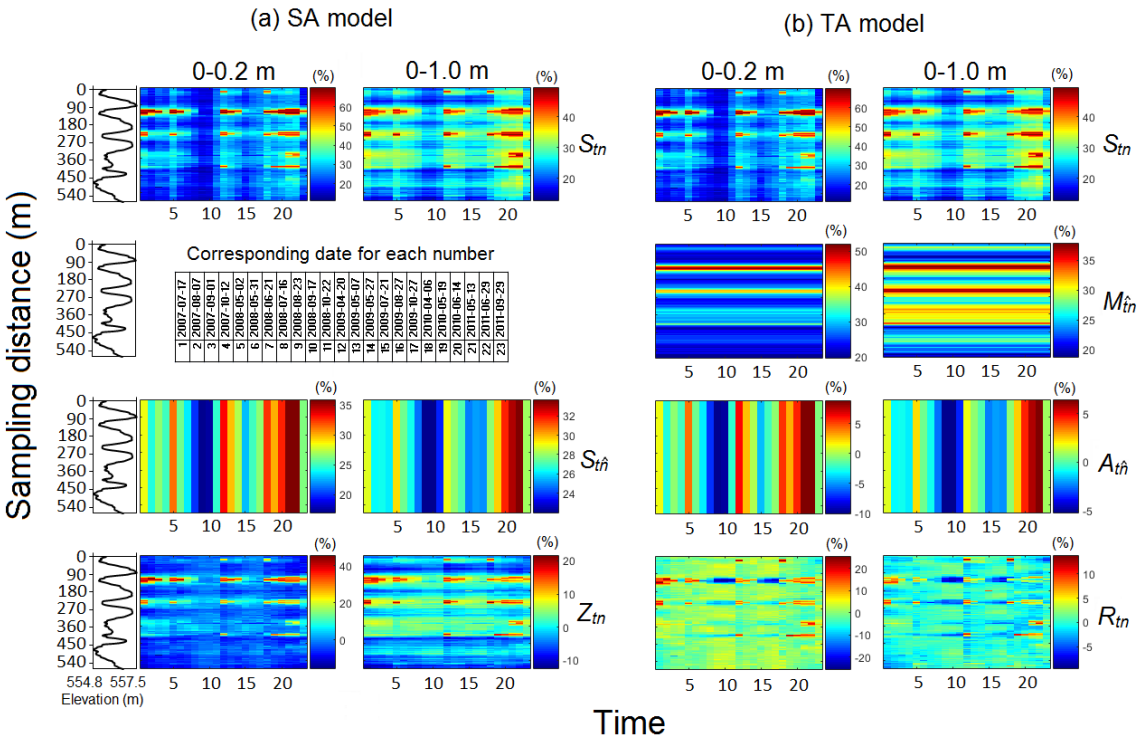


Fig. 3. Components of soil water content in (a) the SA model (spatial mean soil water content $S_{t\hat{n}}$ and spatial anomaly $Z_{tn}$) and in (b) the TA model (time-stable pattern $M_{\hat{t}n}$, space-invariant temporal anomaly $A_{t\hat{n}}$, and space-variant temporal anomaly $R_{tn}$) for 0–0.2 and 0–1.0 m. Also shown is the elevation.

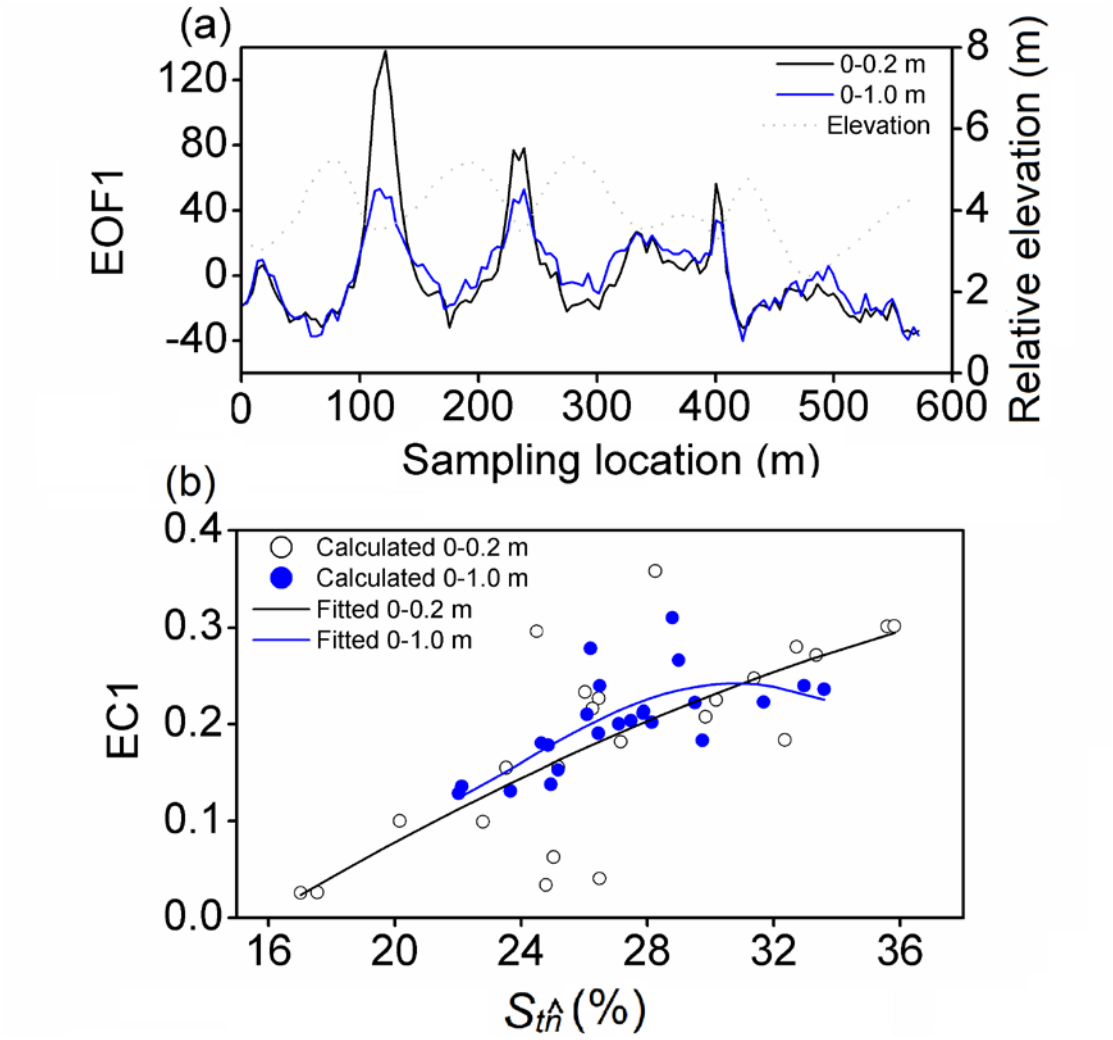


Fig. 4. (a) The EOF1 of the spatial anomaly $Z_{tn}$ and (b) relationships of associated EC1 versus spatial mean soil water content $Z_{tn}$ fitted by the cosine function (Eq. 4).

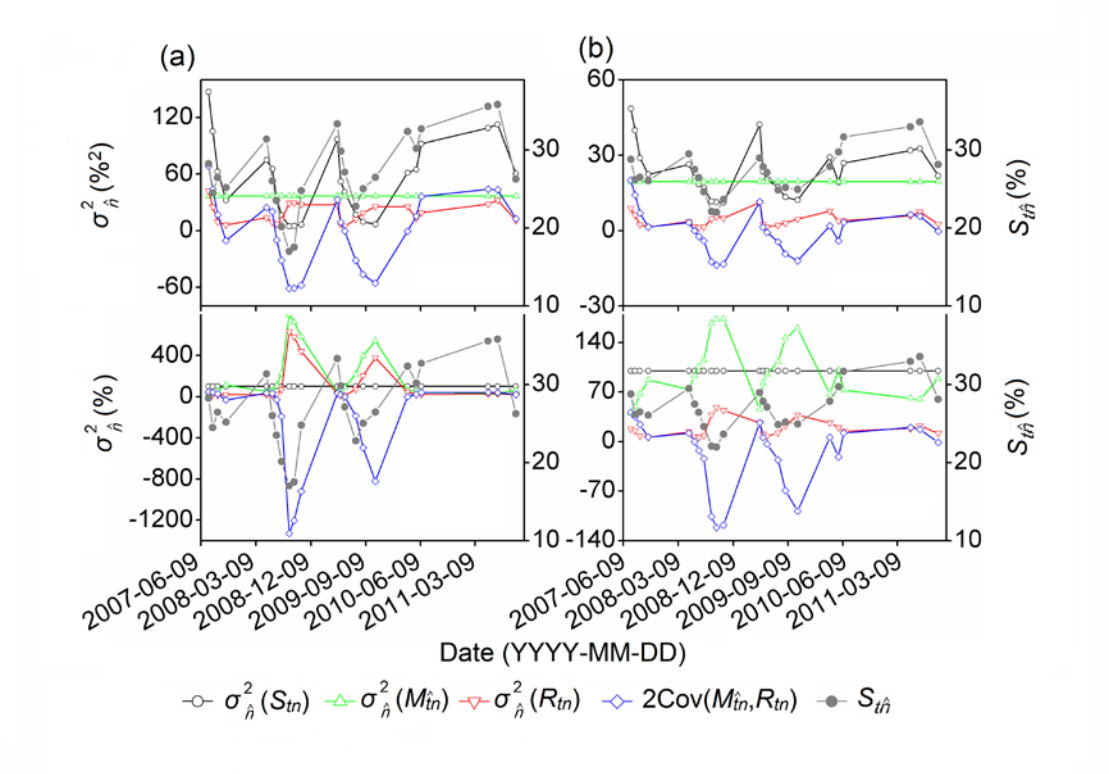


Fig. 5. Spatial variances of different components in Eq. (8) expressed in $\%^2$ (upper panel) and as percentage (lower panel) for (a) 0–0.2 and (b) 0–1.0 m. Spatial mean soil water content $S_{t\hat{n}}$ on each measurement day is also shown.

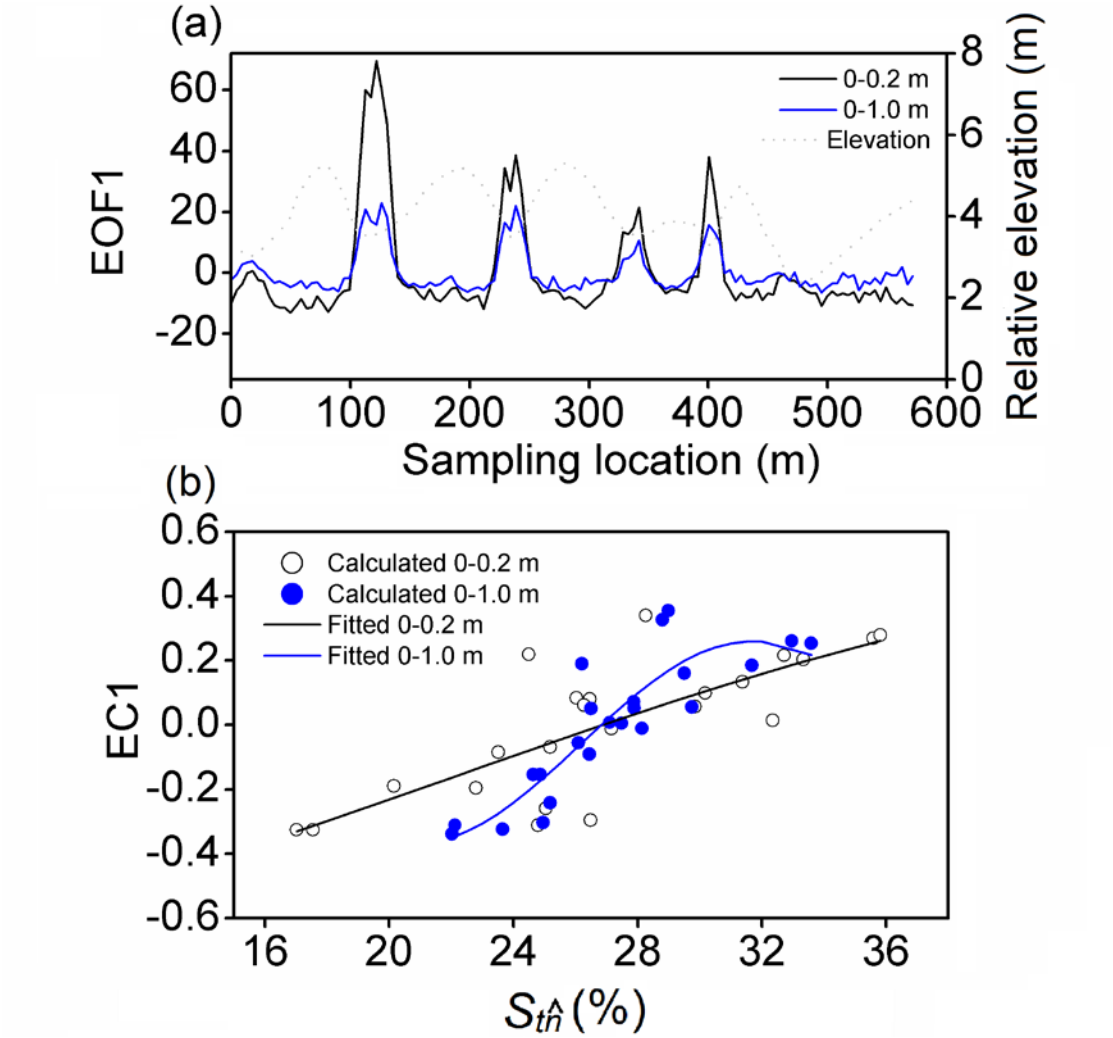


Fig. 6. (a) The EOF1 of the space-variant temporal anomaly $R_{tn}$ and (b) relationships of associated EC1 versus spatial mean soil water content $S_{t\hat{n}}$ fitted by the cosine function (Eq. 4).

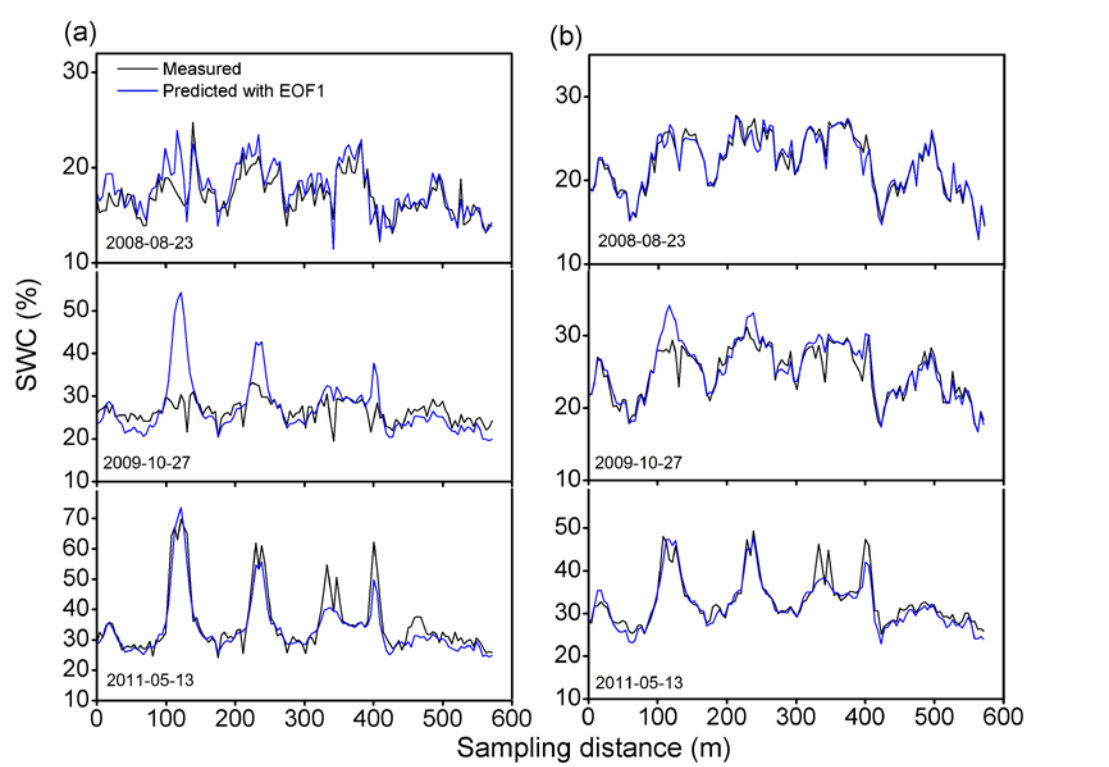


Fig. 7. Estimated soil water content (SWC) versus measured SWC for three dates at different soil water conditions (August 23, 2008, October 27, 2009, and May 13, 2011 are associated with relatively dry, medium, and wet days, respectively) using the TA model for (a) 0–0.2 and (b) 0–1.0 m.

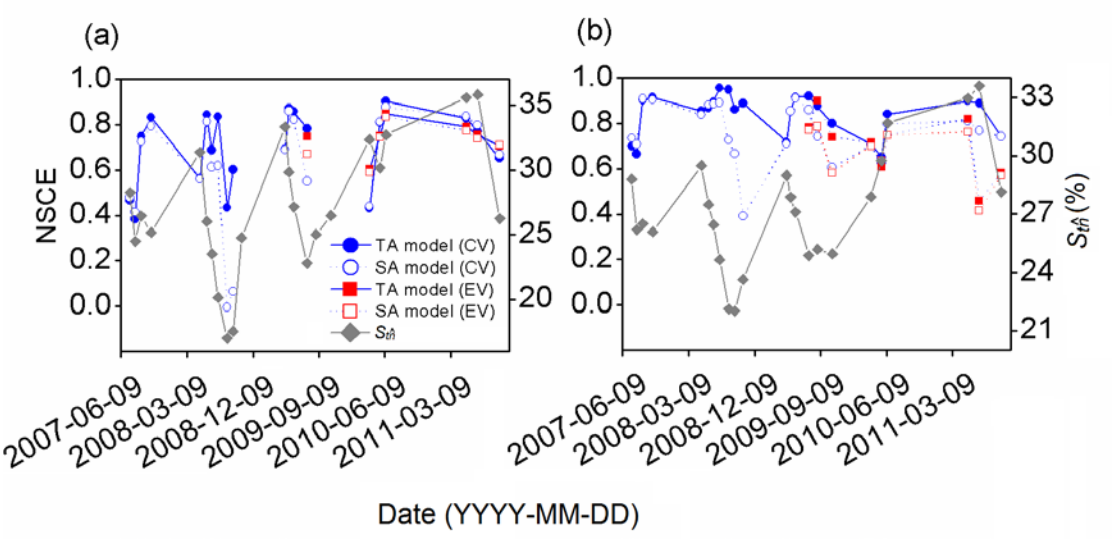


Fig. 8. The Nash-Sutcliffe coefficient of efficiency (NSCE) of soil water content estimation using the TA and SA models for (a) 0–0.2 and (b) 0–1.0 m for both cross validation (CV) and external validation (EV). At 0–0.2 m, negative Nash-Sutcliffe coefficient of efficiency values for three dates (October 22, 2008, August 27, 2009, and October 27, 2009) are not shown. Spatial mean soil water content $S_{t\hat{n}}$ on each measurement day is also shown.

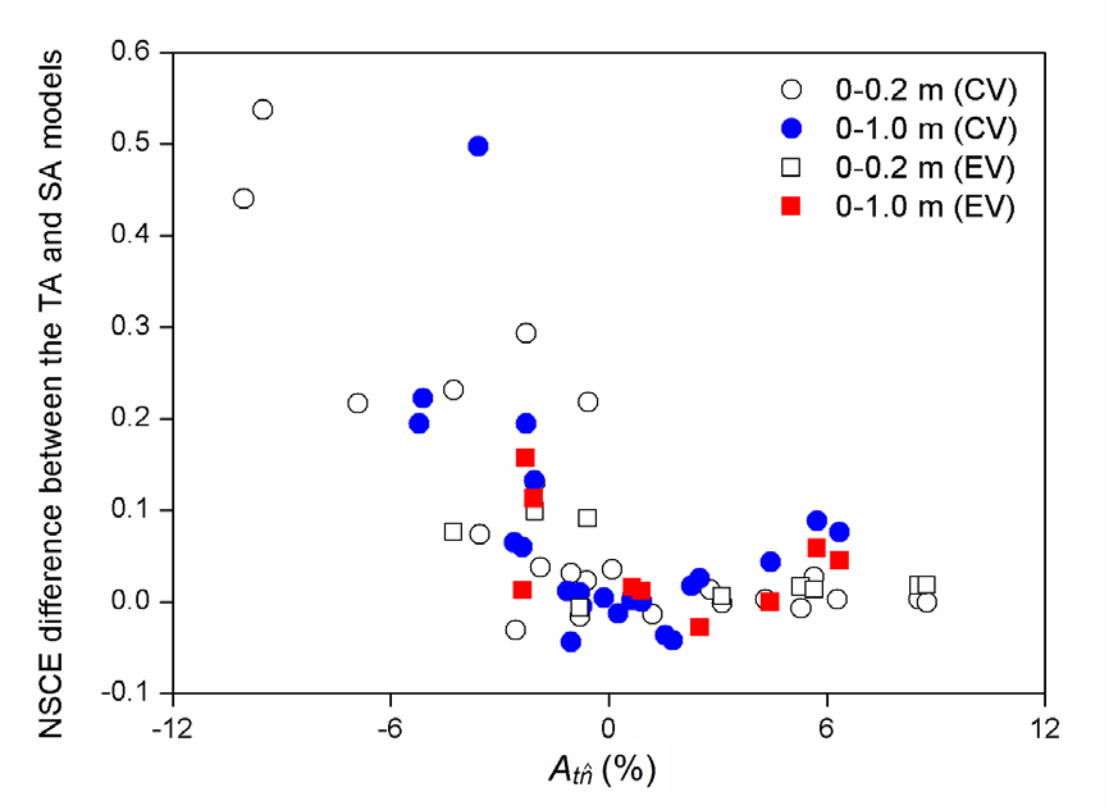


Fig. 9. Difference between the Nash-Sutcliffe coefficient of efficiency (NSCE) of soil water content estimation by both cross validation (CV) and external validation (EV) using the TA and SA models as a function of space-invariant temporal anomaly $A_{t\hat{n}}$ for (a) 0–0.2 and (b) 0–1.0 m.

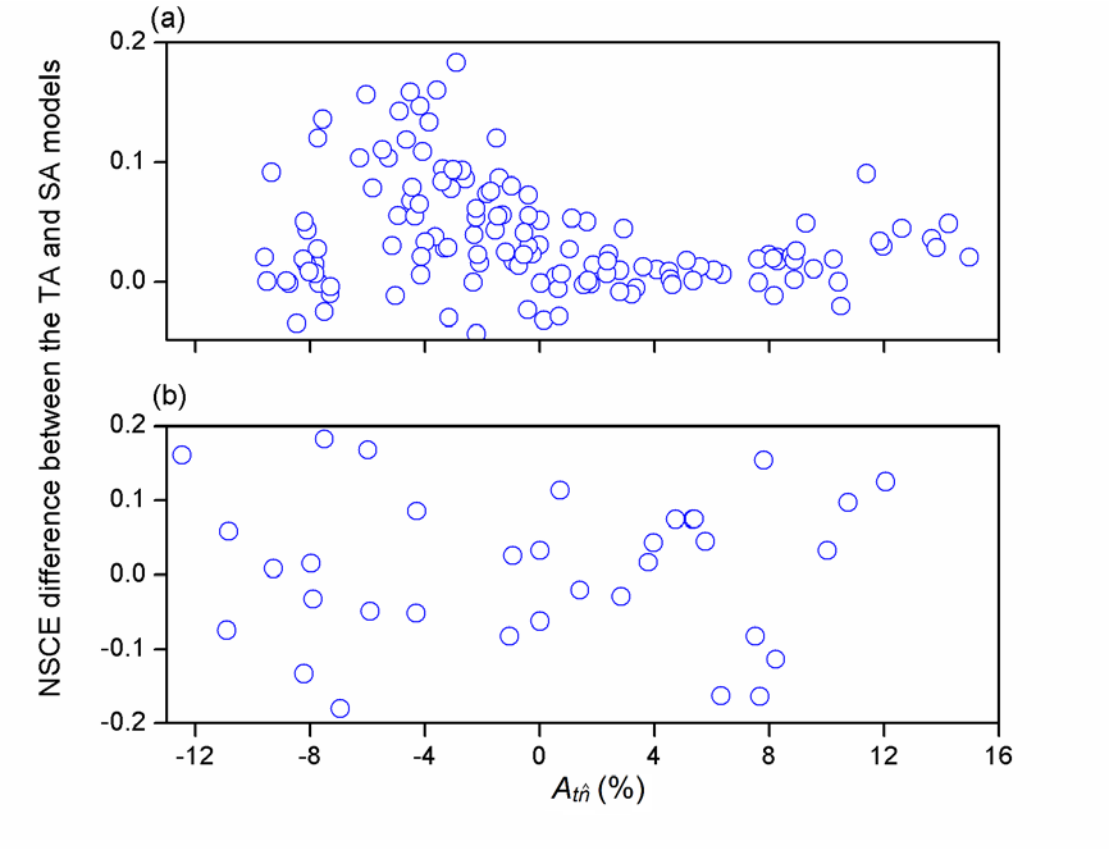


Fig. 10. Difference between the Nash-Sutcliffe coefficient of efficiency (NSCE) of soil water content evaluation by the cross validation using the TA and SA models as a function of space-invariant temporal anomaly $A_{t\hat{n}}$ for (a) 0–0.06 m of the Chinese Loess Plateau hillslope and (b) 0–0.15 m of the GENCAI network in Italy.